Conformal VLC Receivers with Photodetector Arrays: Design, Analysis and Prototype

Pooya Nabavi[1] and Murat Yuksel[1,2]
[1]Department of Electrical and Computer Engineering, University of Central Florida, Orlando, FL USA 32816
[2]College of Optics and Photonics, University of Central Florida, Orlando, FL USA 32816
pooya.nabavi@knights.ucf.edu, murat.yuksel@ucf.edu

***Abstract*—To enable visible light communication (VLC) for mobile receivers, we design and prototype a wide field-of-view (FOV) optical receiver with off-the-shelf components and in forms that are conformal to the receivers' surface. The VLC system uses high-efficiency optical transmitters with high brightness (7645 Lux in 1 m) low power (36 W) white LED panels which also provide proper lighting. To overcome the detrimental effects of the time-varying inter-symbol interference (ISI) due to the VLC receiver's high acceptance angle and vibration in its structure, we design and utilize an optimal multiple-symbol detection (MSD) algorithm. MSD attains remarkable improvements compared to the symbol-by-symbol detection but with exponential time cost. To decrease the MSD's computing demands, we then design an adaptive Decision Feedback Affine Projection Algorithm (DF-APA). DF-APA attains a notable further improvement with polynomial computation complexity which allows faster response to VLC channel dynamics. We, finally, test the system in presence of intense vibration in the receiver's body and show a 20 Mbps VLC link over 7 m distance.**

***Index Terms*—Indoor visible light communications, System design, Vibrant VLC link, Multiple-symbol detection, Adaptive decision feedback affine projection algorithm.**

I. Introduction

Optical wireless communications has brought forward a potential framework for reaching secure, high-throughput, and cost-effective wireless communications in multi-user environments [1], free space and underwater [3]. As the density of Internet-of-Things (IoT) devices is increasing in our living spaces, legacy radio frequency (RF) bands are getting more scarce and expensive to license. Further, due to the interference caused by the omni-directional RF signals, the aggregate wireless network throughput increases sub-linearly [4], and there is an urgent need for more spatial reuse to increase the aggregate wireless network capacity.

Compared to the legacy RF-based wireless communications, VLC has many advantages including higher bandwidth, higher potential for spatial reuse and lower probability-of-intercept. Although these features make VLC a perfect solution for high-throughput indoor wireless networking, a casual office setting involves many dynamics that may hinder the benefits of VLC. The frequent existence of mobility and undesired vibrations caused by regularities of an office setting (e.g., a simple shake from typing on a laptop or movements of smart phone while talking or watching video) may adversely affect the efficient signal reception at a VLC receiver. Such casual operation can cause attenuation and impose a time varying inter-symbol interference (ISI) on the received optical signal, and hence limit the viable communication bit rate and effective range of indoor VLC systems. This impediment hampers on the widespread usage of VLC systems and necessitates intelligent receiver design and efficient transmission and reception methods. However, to the best of our knowledge, the detrimental impacts due to the above mentioned phenomena on the performance of the VLC systems and appropriate solutions yet has not been studied, which is the main focus of this work.

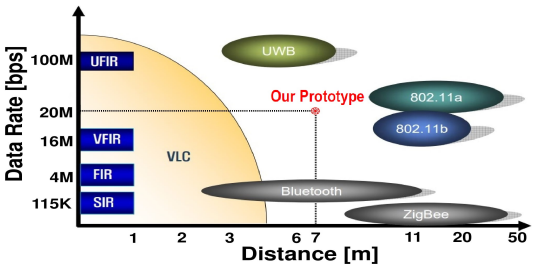

Fig. 1. VLC technology, IEEE 802.15.7 standard [11]

In this paper, we design and prototype a 20 Mbps VLC receiver for indoor office communications with a range of 7 m. We examine the VLC link's performance and stability against mobility and vibration. We measure the channel's delay spread in both presence and absence of the intense vibration in the receiver's structure and quantify the reduction in the maximum achievable rate due to the ISI caused by the vibration. To reduce the ISI, we then design an optimal Multiple-Symbol Detection (MSD) algorithm specifically to remedy the increased Bit Error Rate (BER) due to the adverse effects of the existing ISI. Further, to prevail upon MSD's exponential computing time requirement, we design and deploy an adaptive Decision Feedback Affine Projection Algorithm (DF-APA) and evaluate the system's performance by utilizing this adaptable detection technique. Our VLC receiver design uses multiple photo-detector (PD) arrays, which can be used to cover various shapes, i.e., conformal to the receiver device's shape. Major contributions of our work include:

- A prototype indoor VLC system that is made of off-the-shelf components, and is scalable and suitable in an office environment and capable of communication with data rates up to 20 Mbps, 7 m coverage and bit error rate of less than 10^{-5} in presence of intense vibration (i.e, speed of 0.2 m/s, acceleration of 43.02 m/s^2, displacement of 37.74 mm, and frequency of 6.27 Hz) in receiver's body.
- A multi-photodetector (PD) array VLC receiver design

978-1-5386-8088-9/19/$31.00 ©2019 IEEE

that is conformal to surfaces of IoT shapes (e.g., laptop, TV monitor, or VR headset) and has a large aggregate receiver surface area arranged in a cubical or flat structure for larger FOV and reception range.
- Empirical modeling of an indoor VLC channel for a casual office setting involving minor movements such as shake or vibration.
- Formulation of ISI effects on wide FOV receivers in vibrant VLC channels with high delay spread and non-zero memory. Consideration of vibration in the environment, beam divergence angle, data rate and link range.
- Design of an optimal and adaptive multi-symbol detection algorithm to handle the time-varying nature of the vibrant VLC channel.

II. VLC Receiver Design

There has been major efforts in VLC receiver design. However, VLC receivers are still not widely and commercially adopted. Insufficient efficiency to offer both high speeds (tens of Mbps) [2], [5], [8] and long ranges (at least 5 m) [6], [7] is among the major reasons dissuading users to extensively employ these receivers (Fig. 1). Moreover, the limited field of view (FOV) ($\approx 75^{\circ}$) and detection area ($\approx 1\ \mathrm{mm}^2$) in the existing VLC receivers cause the generated data-carrying photo-current signal to be small and the quality of the data reception to be dependent on the spatial positions of the receiver and transmitter. These limitations make it impossible to broadly implement wide-range VLC systems in environments where the receiving person is constantly on the move. Table I details the performance of the state of the art VLC technologies [1]. By making the VLC receivers conformal, we focus on design and implementation of wide FOV receivers and show a maximum omni-directional reception rate of 20 Mbps at a range of 7 m.

A. Biasing Circuit

A PD signal can be measured as voltage or current. The PD current measurement demonstrates far better linearity, offset, and bandwidth performance. The generated photo-current is proportional to the incident light power and it must be converted to a voltage using a transimpedance configuration. The PD can be operated with or without an applied reverse bias ($\mathrm{V_B}$) depending on the application-specific requirements. Application of a reverse bias (i.e., cathode positive, anode negative) can greatly improve the speed of response and linearity of the devices. In our configuration, the detector is reverse biased to reduce PD's total junction capacitance, thus reducing its rise time, $\mathrm{t_r}$. Moreover, the reverse biasing technique was employed through active TIA in order to eliminate the dependency between the voltage of the PD's cathode pin and the feedback resistor, $\mathrm{R_F}$, responsible for converting voltage to current. As shown in Fig. 2, the cathode pin is connected to the inverting pin of the operational amplifier which has the same zero voltage as its non-inverting pin. As one of the advantages of this structure, the voltage difference between the two PD pins is independent of the undesirable variations of $\mathrm{R_F}$ caused by the changes in the ambient temperature. This, in turn, leads to further independence of the receiver bandwidth from the temperature conditions in indoor office environments, consequently reducing the maximum communication range.

TABLE I
Performance Comparison

	R	BW	FOV	Packet Loss Rate
Our Prototype	7.1 m	20 MHz	360°	10^{-6}
Pure LiFi-X [6]	1.8 m	42 MHz	60°	$\approx 3.4 \times 10^{-5}$
[5]	2.4 m	10 KHz	10°	10^{-2}
[2]	50 m	50 KHz	75°	3.2×10^{-4}
Thorlabs [7]	0.45 m	12 MHz	150°	$\approx 10^{-4}$

[1]Note that for providing proper lighting coverage, the technologies listed in Table I utilize white Phosphorus LEDs (not single wavelength LDs) as their predominant choice for data transmission. These white phosphorous LEDs have limited oscillation/switching frequency ($\approx$ 50 MHz) and as a result of that, the maximum transmission bit rate without using code division multiple access (CDMA) coding techniques is limited to maximum 50 Mbps. However, by utilizing monotonic (single wavelength) LEDs we can reach Gbps speeds [9] but we will not be able to provide proper lighting coverages.

The overall bandwidth (BW) of the receiver is directly determined by $\mathrm{R_F}$ as follows [10]:

$$\mathrm{BW}\ [Hz] = \sqrt{\frac{\mathrm{GBP}}{2\pi \times \mathrm{R_F} \times (\mathrm{C_J} + \mathrm{C_F})}} \tag{1}$$

where GBP is the gain bandwidth product of the operational amplifier (OPA637BP) and is equal to 80 MHz, $\mathrm{C_F}$ is the feedback phase-compensation capacitor, $\mathrm{C_J}$ is the equivalent junction capacitance of the cubical structure.

B. Three-Stage Voltage Amplification

Amplification of the received signal with a high gain while maintaining stability is very important in order to provide a long VLC communication range. Existing amplification of PD signals involves only a simple TIA designed for low-speed operation and uses high feedback resistor $\mathrm{R_F}$ to attain high gain. But, high $\mathrm{R_F}$ limits the bandwidth, and such designs are not appropriate for our VLC goals with large surface area PDs operating at high speeds. In order to maintain wide bandwidth, high gain and long communication range, we amplify and detect our data-carrying signal through three stages. The three stages include a transimpedance pre-amplification for current-to-voltage conversion (Stage 1, $\mathrm{G_{TIA}}$) and a non-inverting amplifier for voltage amplification (Stage 2). Between these two stages we use a high pass filter. As shown in Fig. 2, we further follow the wide bandwidth amplification of Stage 2 with a wideband pulse amplifier (Stage 3, $\mathrm{G_{WBA}}$) which provides a 30 dB gain at a 500 MHz bandwidth.

C. Gain - Bandwidth trade off

Finding the right value for the feedback capacitance $\mathrm{C_F}$ involves tuning its trade off with phase margin and bandwidth. Higher $\mathrm{C_F}$ means more stability (i.e., large phase margin) but less bandwidth. In this design, we target 45° of phase margin (i.e., 180° + $\angle \mathrm{A_v(f_i)}\beta(\mathrm{f_i}) = 45^{\circ}$ where f_i, $\mathrm{A_v(f)}$ and $\beta(\mathrm{f})$ are the intercept frequency, TIA's open loop gain and its feedback factor, respectively.). The 45° phase margin provides a good compromise between stability and bandwidth, and enables us to obtain a closed-form $\mathrm{C_F}$:

$$\mathrm{C_F} = \frac{1 + \sqrt{1 + 4.8\pi \times \mathrm{R_F} \times \mathrm{C_J} \times \mathrm{GBP}}}{2.4\pi \times \mathrm{R_F} \times \mathrm{GBP}}. \tag{2}$$

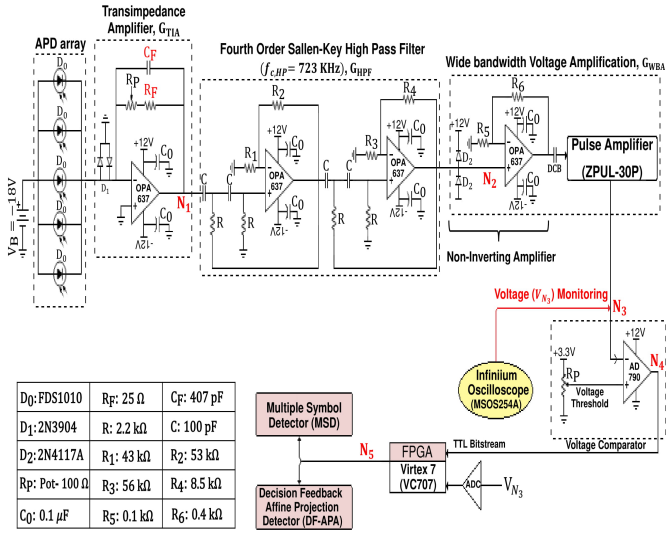

Fig. 2. VLC receiver circuit

In order to make sure the biasing circuit does not become a bottleneck to the VLC receiver's BW, we need to select the feedback resistor R_F as large as possible (for high gain) while not limiting the maximum achievable BW of the PD FDS1010. To respect the BW of the PD, we must satisfy BW $[Hz] \geq f_{PD,3dB}$, where $f_{PD,3dB} \approx \frac{0.35}{t_r}$ is the frequency at which the PD output decreases by 3dB and is equal to 19.85 MHz when t_r is 18 ns measured at $V_B = 18$ V. By substituting Eq. (2) in Eq. (1) and solving BW $[Hz] \geq 19.85$ $[MHz]$, we find the maximum value of R_F as 25 Ω, Finally, by substituting $R_F = 25$ Ω in Eq. (2), C_F calculates to 407 pF.

III. VLC Prototype and Results

The prototype and experimental setup for the VLC receiver and transmitter are demonstrated in Fig. 3. In order to evaluate our receiver in presence of vibration, we assembled the entire body of the receiver's structure on a servo motor. We employ an Arduino to control the speed and direction of the servo, which enables us to produce an intense vibration pattern with our desired characteristics (i.e. frequency, acceleration, velocity, and displacement) in the body of the receiver. Finally in order to study the effects of vibration on the reception quality, we plotted the eye diagram of the received signal at transmission rate of 20 Mbps in presence and absence of vibration respectively.

A. Inter-Symbol Interference

Real-time eye diagrams in Fig. 5 provide instant visual data that can be used to check the prototype's signal integrity in both presence (Fig. 5(d)) and absence of vibration (Fig. 5(c)). We also characterized and measured the vibration intensity of the considered indoor office setting, for both vibrant (Fig. 5(b)) and non-vibrant (Fig. 5(a)) VLC links. As shown in Fig. 5(d)), the increased ISI[2] creates distortion and eye closure.

[2]Note that although these PD arrays increase the FOV to 360°, they also increase the ISI. Consequently, the average BER, particularly at high bit rates, also increases when deployed in a vibrant mobile VLC link. We will address these challenges in Sections IV and V.

B. Channel Impulse Response

Understanding the effect of vibration on the VLC channel is crucial and, to the best of our knowledge, has not been empirically done before. From our prototype, we measure the channel impulse response to calculate the approximate delay spread of the VLC channel in both presence and absence of vibration (Fig. 4). High delay spread indicates the amount of ISI in the channel, and thus, tells a lot about the channel quality. To empirically measure the impulse response, we sent a 5μs high signal from the transmitter and stored V_{N_2} in a buffer. The stored V_{N_2} is proportional to the intensity of the incident light radiated on the PD. Finally, assuming linearity in the channel behavior, we estimated the channel impulse response by calculating the inverse FFT of the ratio of the FFT of V_{N_2} to the FFT of transmitted high signal of width 5μs. We also calculated the channel's RMS delay spread in both presence and absence of vibration using [3]:

$$\tau_{\mathrm{RMS},i} = \sqrt{\frac{\int_{-\infty}^{\infty}(t-\tau_i)^2 h_i^2(t)\mathrm{d}t}{\int_{-\infty}^{\infty} h_i^2(t)\mathrm{d}t}}, \quad i = 1,2 \qquad (3)$$

where τ_i is the mean delay due to non-LOS paths and is given by $\tau_i = \int_{-\infty}^{\infty} h_i^2(t)t\mathrm{d}t \Big/ \int_{-\infty}^{\infty} h_i^2(t)\mathrm{d}t$, i=1,2. Here, $h_2(t)$ and $h_1(t)$ are the estimated impulse responses for the VLC channel with or without vibration, respectively. By Eq. (3), we estimate the effective delay spread $\tau_{\mathrm{RMS},1}$=312.34 ns and $\tau_{\mathrm{RMS},2}$=7.04 ns over 7 m.

IV. Multiple-Symbol Detection

Drawing on the experimental results, we obtained the impulse response of the VLC channel in the previous section (Fig.4), revealing that the delay spread of the channel drastically increases in the presence of the intense vibration in the receiver. The delay spread interrupts the symbols transmitted on the channel and deteriorates the overall performance of the optical system, which in turn limits the communication range. In this section, we design an optimal detector, aiming to restore the performance lost in symbol-by-symbol detection due to the ISI in which detection decisions are made using a multi-bit observation window.

A. System Model

On transmitter side, we have assumed intensity modulation direct-detection with On-Off Keying (OOK) modulation, i.e., 1s represented with high light intensity and 0s with low. As a result, the transmitted data sequence of the transmitter can be expressed as:

$$x(t) = \sum_{m=0}^{\infty} b_m P(t - kT_b) \qquad (4)$$

where $T_b = \frac{1}{R_b}$ is the bit duration time and R_b is the data transmission rate. Moreover, in this scheme, bits "0" and "1" of each time slot will be transmitted with pulse shapes 0 and rectangular pulse $P(t)$ with time duration of T_b, respectively, and $b_m \in [0,1]$ is the OOK modulated signal corresponding to the m^{th} transmitted bit (or symbol).

On the receiver side of the VLC system, the output data-carrying analog signal (i.e., V_{N_3} in Fig. 2) is integrated over

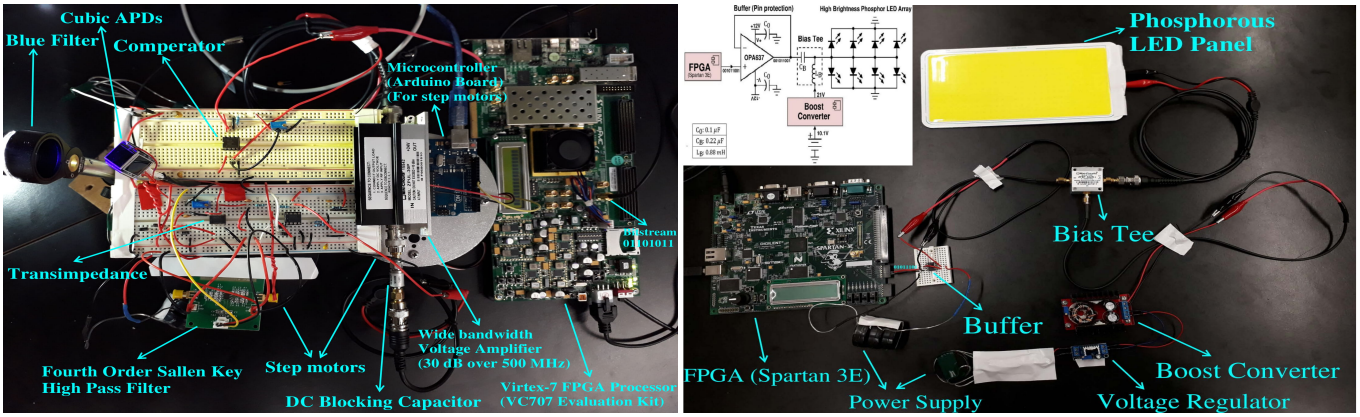

(a) (b)

Fig. 3. VLC prototype: (a) Receiver; (b) Transmitter.

consecutive bit times (i.e., $\int_{kT_b}^{(k+1)T_b} V_{N_3}(t)\mathrm{d}t$) and as a result a discrete signal is built in each time slot, i.e., $r(k)$ where k indicates the index of the time interval at which k$^{\text{th}}$ transmitted bit is integrated. When a photon hits a PD, the generated output photo-current of the PD (i.e., the total number of generated photo-electrons) obeys a Poisson distribution [3]. The output of the integrator can be modeled as a Poisson Point Process whose average is in proportion with the total optical incident power [3]. The integrated output of the optical detector can be modeled as:

$$r(k) = y(k) + \nu_{b,d}(k) \tag{5}$$

where $\nu_{b,d}(k)$ is the Poisson noise (including background and dark current noises) during the detection of the k^{th} symbol in the receiver. $\nu_{b,d}(k)$ is a Poisson variable with an average value of $(n_b + n_d)T_b$, where $n_b = \frac{2\eta_Q \eta_E P_{BG} T_b}{hf}$ and $n_d = \frac{2I_{dc}BT_b}{q}$ are the number of photo-electrons generated by the background light and the dark current noise, respectively. Here, η_Q represents the quantum efficiency of the PD, η_E is the elimination factor of the high-pass filter in our receiver, B is the overall electronic bandwidth provided by our prototype and was obtained in Eq. (1), P_{BG} is the received background power and I_{dc} is the dark current of PD hardware. $q = 1.602 \times 10^{-19} C$ is the elementary charge, $h = 6.626 \times 10^{-34}$ is Plank's constant, and f represents the frequency of the light source. $y(k)$ is the count of photo-electrons generated from the received data-carrying signal, and is also a Poisson variable with an average in proportion to the PD output in the k^{th} interval. By considering the effects of the L detected symbols prior to detection of the k^{th} symbol on increasing the resulting average number of photo-electrons on the k^{th} interval, $y(k)$'s expected value will be:

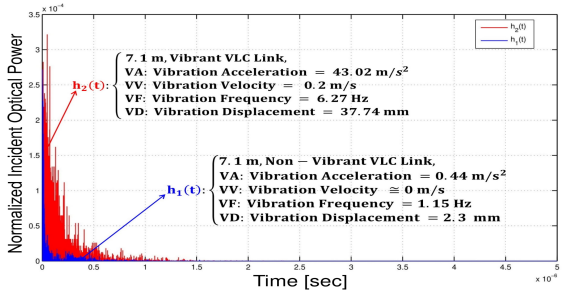

Fig. 4. Channel impulse responce for 7.1 m vibrant and non-vibrant links.

$$m_y(k) = \frac{\tilde{\mathcal{R}}\tilde{h}}{q} \sum_{m=k-L}^{k} b_m \int_{(k-m)T_b}^{(k-m+1)T_b} \Gamma(t)\,\mathrm{d}t \tag{6}$$

where $\tilde{\mathcal{R}}$ is the responsivity of the cubical PD at the corresponding wavelength of the incident light ($\lambda = 445$ nm, Blue color), and $\tilde{h}$ is a positive multiplicative fading coefficient (to characterize turbulence effects). Further, $\Gamma(t) = h(t) * P(t)$ where $h(t)$ is the impulse response of the vibrant VLC channel (which we empirically estimated in Fig. 4) and L is the channel memory which increases with the vibration intensity, data rate, transmitter beam divergence angle, receiver FOV, and distance. Eqs. (5) and (6) imply that $r(k)$ is a Poisson variable with an average $m(k)$ defined by

$$m(k) = \tilde{m}(k)\tilde{h} + (n_b + n_d)T_b \tag{7}$$

where $\tilde{m}(k)$ is defined according to

$$\tilde{m}(k) = \frac{\tilde{\mathcal{R}}}{q} \sum_{m=k-L}^{k} b_m \int_{kT_b}^{(k+1)T_b} \Gamma(t - mT_b)\,\mathrm{d}t. \tag{8}$$

To achieve an optimal decision metric for VLC receiver, we obtain the joint probability distribution function of the $r(0)$, $r(1)$, …, $r(N-1)$ as

$$M_{MSD}(\underline{b}) = \frac{1}{2^L} \times \prod_{i=0}^{N-1} \sum_{b_{i-1},..,b_{i-L}} \left[\int_0^{\infty} Poiss(\, r(i) |\, b_i, (b_{i-1}, .., b_{i-L}), \tilde{h}_i) f(\tilde{h}_i)\, \mathrm{d}\tilde{h}_i \right], \tag{9}$$

where N is our desired window length and $\tilde{h}_i$ is a random variable with Erlang distribution

$$f(\tilde{h}_i; \lambda_F, \theta_F) = \frac{\lambda_F^{\theta_F}}{(\theta_F - 1)!} \tilde{h}_i^{\theta_F - 1} e^{-\lambda_F \tilde{h}_i}, \quad \tilde{h}_i \geq 0. \tag{10}$$

In Eq.(10), $\lambda_F \in \mathbb{R}$ and $\theta_F \in \mathbb{Z}^+$ are selected so that the Erlang function conforms to the normalized Lognormal function with a variance of $\sigma^2_{\tilde{h}_i}$ and mean value 1 [13] which is the typical case in VLC indoor links. By substituting Eq. (10) in Eq. (9), we obtain our optimum decision metric as

$$M_{MSD}(\underline{b}) = \frac{1}{2^L} \times \frac{((n_b + n_d)T_b)^{r(i)}}{r(i)!} \times \frac{\lambda_F^{\theta_F} e^{-(n_b+n_d)T_b}}{(\theta_F - 1)!} \times \prod_{i=0}^{N-1} \sum_{b_{i-1},..,b_{i-L}} \frac{e^{\mu\nu} g_{\theta_F - 1}(r(i); \mu(i), \nu(i))}{\nu(i)(\mu(i)\nu(i))^{r(i)}} \tag{11}$$

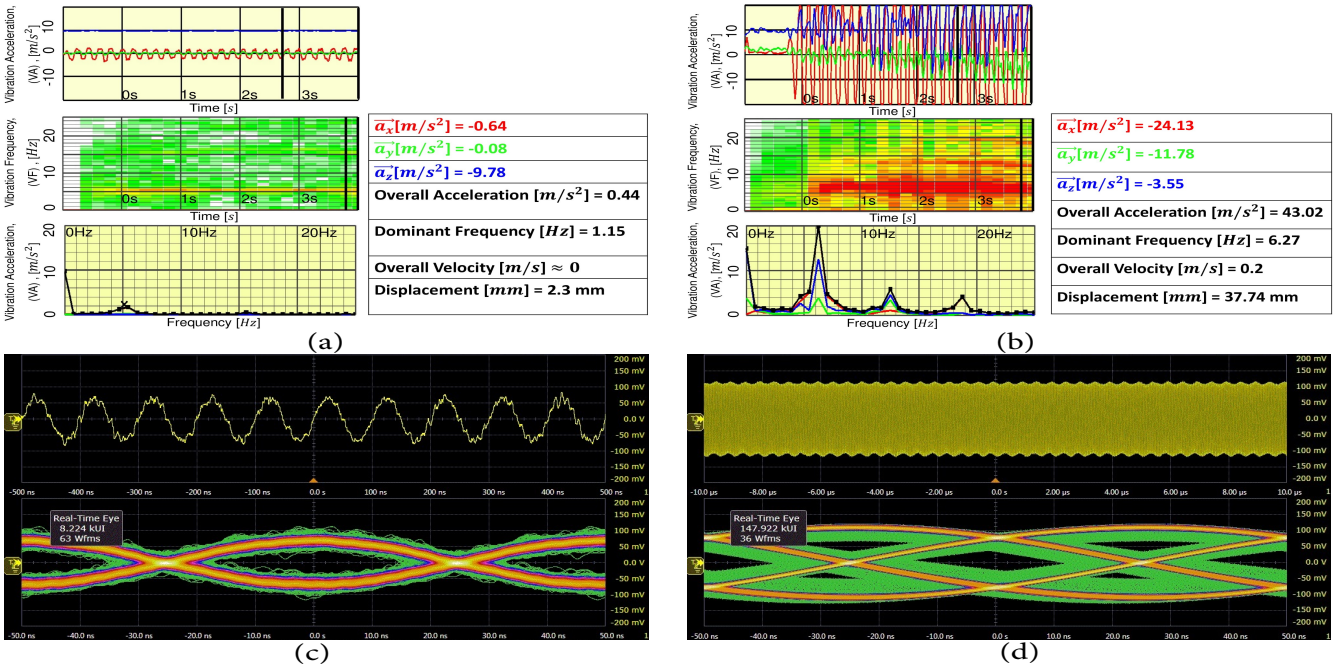

Fig. 5. Eye diagrams for both vibrant and non-vibrant, 7.1 m long VLC link: (a) Vibration conditions when communicating in a non-vibrant VLC link and (b) vibrant VLC link when step-motor (400 R.P.M.) operates, (c) Eye diagram for the 20 Mbps transmission data rate in a non-vibrant and (d) vibrant (speed of 0.2 m/s, acceleration of 43.02 m/s^2, displacement of 37.74 mm, and frequency of 6.27 Hz) VLC link.

where $g_\theta(a;b,c) = c^{a+1}\int_0^\infty x^\theta(x+b)^a e^{-c(x+b)}\mathrm{d}x$, $\nu(i) = \tilde{m}(i) + \lambda_F$, $\mu(i) = \frac{(n_b+n_d)T_b}{\tilde{m}(i)}$ and $b_{-1}, b_{-2}, \ldots, b_{-L}$ are assumed 0. Further, the sum symbol $\sum_{b_{i-1},b_{i-2},\ldots,b_{i-L}}$ is used to define the summation over all possible binary sequences for $b_{i-1}, b_{i-2}, \ldots, b_{i-L}$. The division of the resulting sum by $\frac{1}{2^L}$ leads to the average value over all possible bit combinations. Since only the last term in Eq. (11) includes the detected bits b_is, the receiver needs to consider only that term for optimal decision on what bits were transmitted. Thus, the optimal receiver must select a bit vector from the 2^N possible bit vectors $\underline{\hat{b}} = [b_0, b_1, \ldots, b_{N-1}]$. It will do so by solving the following maximization problem:

$$\underline{\hat{b}}_{N\times 1} = \underset{\underline{b}}{\operatorname{argmax}} \prod_{i=0}^{N-1} \sum_{b_{i-1},..,b_{i-L}} \frac{e^{\mu(i)\nu(i)} g_{\theta_F-1}(r(i);\mu(i),\nu(i))}{\nu(i)(\mu(i)\nu(i))^{r(i)}} \tag{12}$$

where L represents the channel memory. In Section VI, we exhaustively search all possible bit vectors which incurs a computational complexity of $O(2^N)$. Next, we design a prediction algorithm to relieve this complexity.

V. Adaptive Symbol Detection

In this section, we design and analyze a two-mode operational adaptive detector, namely, "Decision Feedback - Affine Projection Algorithm" (DF-APA) to tackle the ISI problem. This approach lends itself well to mixed-signal designs that can attain similar performance to the optimum MSD techniques. Moreover, the adaptive detector discussed in this section offers a considerably lower computational complexity with a polynomial order.

A. System Model

The main idea behind decision feedback detectors is that when the data symbol is detected and decided, one can obtain and eliminate ISI on the future symbols prior to detection of the next symbols. This algorithm can be constructed as a feed forward (FF) filter and feedback (FB) filter in the optical receiver. ISI created by previously detected symbols on the current symbol can be adjusted using FB filter coefficients. Detector consists of N_{FF} + 1 taps in its FF filter and N_{FB} taps in its FB filter. As shown in Fig. 6, the adaptive system works in two modes, i.e, training and tracking modes, to detect the transmitted symbols. When in the training mode, the detector's output $\hat{d}_k$ will be equal to $\underline{\omega}^T(k)\underline{u}(k)$, where $\underline{u}(k) = [r(k) \ \ldots \ r(k-N_{FF}) \ d_{k-1} \ \ldots \ d_{k-N_{FB}}]^T$ is the input signal of the detector seen in Fig. 6, $\underline{\omega}(k) = [\omega_0 \ \omega_1 \ \omega_2 \ \ldots \ \omega_{(N_{FF}+N_{FB})}]^T$ represents the impulse response of the overall discrete adaptive filter containing both FF and FB tap weight coefficients after being updated for k times, $\omega_{i=0,\ldots,N_{FF}+N_{FB}}$ are the gain coefficients (taps) used in the detector and d_i is the input training sequence. Based on the conventional protocol between the transmitter and receiver, the training sequence bits d_i can be made available in the transmitted preamble packets, allowing the receiver to have full knowledge of these preamble bits and have full access to the training sequence. By obtaining the detector's output $\hat{d}_k$, the error signal e_k is determined using $d_k - \hat{d}_k$ and $\tilde{d}_k - \hat{d}_k$ in the training and tracking modes, respectively. Here, $\tilde{d}_k$ can be computed as

$$\tilde{d}_k = \begin{cases} 1 & \hat{d}_k \geq \mathrm{V_{Th}} \\ 0 & \hat{d}_k < \mathrm{V_{Th}} \end{cases} \tag{13}$$

where $\mathrm{V_{Th}}$ is the voltage threshold and is the average output voltage over multiple symbols. This method eliminates the need for channel state information in the receiver for generating the training sequence in tracking mode. The error signal

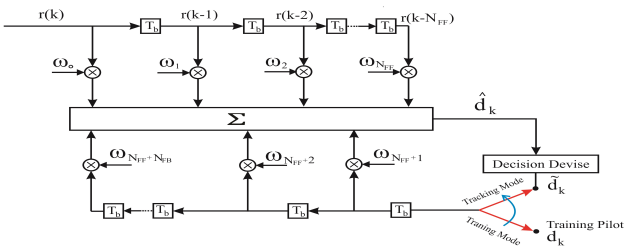

Fig. 6. DF-APA structure

is squared to obtain the mean square error at the instant of k, leading to

$$J(k) = E\{|e_k|^2\} \tag{14}$$

where $J(k)$ is the cost function at the instant of k.

Adaptive symbol detectors requires a special algorithm to update the detector coefficients and thus minimize the desired cost function. There exists a wide variety of adaptive algorithms updating filter coefficients. Here, we use Affine Projection Algorithm (APA) [12] to update the tap weight vector coefficients $\underline{\omega}(k)$. In the following subsection, the proposed algorithm is described in detail.

B. Configuring the Adaptive Filter

Given the set of tap-input vectors $\underline{u}(k)$, $\underline{u}(k-1)$, $\ldots$ $\underline{u}(k-(N_{FF}+N_{FB})+1)$ and the set of desired output samples d_k, d_{k-1} $\ldots$ $d_{k-(N_{FF}+N_{FB})+1}$, the tap-weight vector $\underline{\omega}(k+1)$ will be updated so as to minimize the squared Euclidean norm of the difference $\underline{\omega}(k+1)$-$\underline{\omega}(k)$ subject to $\underline{\omega}^T(n+1)\underline{u}(n-i) = d_{n-i}$ for $i = 0,\ 1, \ldots M-1$ as a sets of constraints. Here, M is the number of applied constraints (i.e., dimensions). By increasing M, the convergence speed increases. However, this increase is limited by a threshold, after which its effect is negligible and further increment of M adds to the computational complexity. Note that NLMS algorithm is a special case of APA for M=1. In our DF-APA design, both in training and tracking modes, we set M=2 to increase the convergence speed compared to the common NLMS algorithm while maintaining the computational complexity at a moderate level. To update the tap weight vector in DF-APA, we formulate the following recursive optimization problem:

$$\min \qquad \|\underline{\omega}(n+1) - \underline{\omega}(n)\|^2 \tag{15}$$
$$S.t. \begin{cases} \underline{\omega}^T(n+1)\underline{u}(n) = d_n \\ \underline{\omega}^T(n+1)\underline{u}(n-1) = d_{n-1}. \end{cases}$$

This optimization problem can best be solved using Lagrange multipliers [15], for which a recursive solution equation can be written as

$$\underline{\omega}(n+1) = [\mathrm{I} - \mu \mathrm{A}^T(n)[\mathrm{A}(n)\mathrm{A}^T(n)]^{-1}\mathrm{A}(n)]\underline{\omega}(n) + \mu \mathrm{A}^T(n)[\mathrm{A}(n)\mathrm{A}^T(n)]^{-1}\underline{d}(n) \tag{16}$$

where μ is the step size for controlling the algorithm's overall stability and convergence speed, $\mathrm{A}^T(n) = [\underline{u}(n),\ \underline{u}(n-1),\ \ldots,\ \underline{u}(n-M+1)]$ and $\underline{d}^T(n) = [d_n,\ d_{n-1},\ \ldots,\ d_{n-M}]$ and M=2. The computational cost of solving Eq. (22) is $O(M(N_{FF}+N_{FB}))$ per sample (iteration) [12].

TABLE II
COMPLEXITY OF SYMBOL DETECTION.

Algorithm	DF-APA	MSD	SBSD
Memory	$O(N_{FF}+N_{FB})$	$O(N)$	$O(1)$
Computation	$O(M(N_{FF}+N_{FB}))$	$O(2^N)$	$O(1)$

VI. RESULTS AND DISCUSSION

We aim to compare our prototype's performance with the optimal MSD and adaptive symbol detection (DF-APA) techniques. Our prototype uses Symbol by Symbol Detection (SBSD) while MSD and DF-APA perform additional computation to improve the BER of the VLC link. This comparative evaluation will reveal the benefit of computation in tackling the performance degradation of the receiver's vibration in the VLC link. At a high level, Table II details the memory and computation complexities of the three symbol detection techniques. SBSD is the baseline approach in our prototype which makes detection for every symbol without spending any additional memory or computation. On the other end of the design spectrum, MSD finds the optimum detection for every N bits with an exponential time and linear memory complexity. The adaptive filtering technique DF-APA, which is a commonly used machine learning method for digital signal processing, finds a middle-ground by attaining linear time and memory complexity with some degradation of BER. In our evaluation, we aim to quantify this degradation too. By using the empirical channel impulse response of our prototype VLC link, we simulate SBSD, MSD and DF-APA. Table III summarizes key system parameters in the simulation, including the transmitter and receiver specifications.

1000X BER Improvement is Possible: By employing the MSD optimal detector in the receiver, we investigate the effect of increasing the window length N on improving the performance of the vibrating receiver at a bit rate of 20 Mbps. Since the highest detrimental ISI effects occur at this bit rate, we choose this particular bit rate for evaluation. Moreover, we are mainly interested in the performance of the MSD optimal detector in improving the detection efficiency under the worst conditions which in our case happens at 20 Mbps over 7.1 m distance. As shown in Fig. 7(a), increasing the window length in the MSD detector from N=2 to N=7 significantly decreases the average BER. Further increases in the window length ($N \geq 8$) have no notable effect on the performance and merely increases the computational complexity and the required buffer for storage of received signal symbols while delaying the decisions on the most probable transmitted N-bit.

TABLE III
SYSTEM PARAMETERS USED IN SIMULATIONS.

Coefficient	Value
Responsivity at $\lambda = 445$ nm, $\tilde{\mathcal{R}}$	0.13
$\mathrm{G_{TIA}}, \mathrm{G_{HPF}}, \mathrm{G_{WBA}}$ (Fig. 2)	$25, 2.57, 5000$
Quantum efficiency, η_Q	0.7
HPF elimination factor, η_E	10^{-6}
Electronic bandwidth, B (Eq. (1))	20.16 MHz
Optical blue filter bandwidth (Full Width Half Max), $\triangle\lambda$	40 ± 8 nm
Optical filter transmissivity at $\lambda = 445$ nm, T_F	0.76
Dark current, I_{dc} at $\mathrm{V_B} = 18V$	80 μA
Transmission bit rate, $\mathrm{R_b}$	20 Mbps
Center-to-center LoS distance between transmitter and receiver	7.1 m
Channel memory, L	7
$\{\lambda_\mathrm{F}, \theta_\mathrm{F}\}$ [14]	$\{6.472, 6\}$

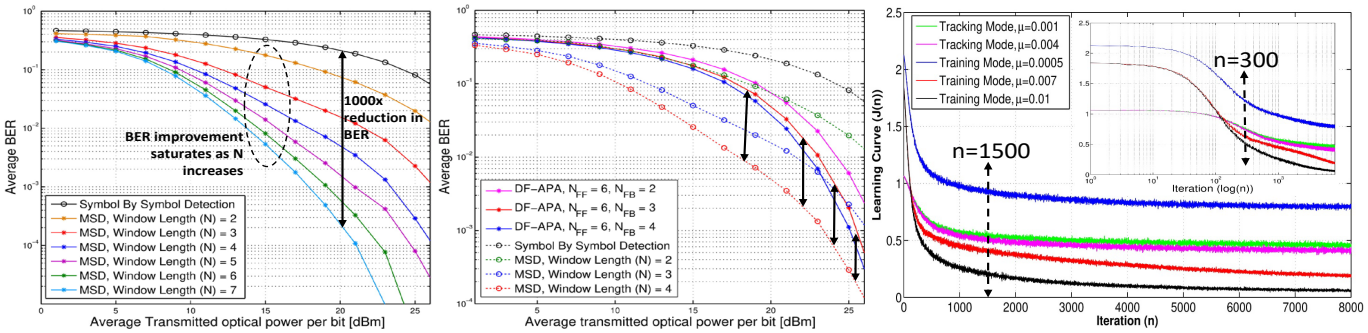

Fig. 7. Performance analysis of a 20 Mbps vibrant VLC link at 7.1 m distance: (a) BER of the optimal MSD receiver at varying window lengths; (b) BER Comparison between suboptimal DF-APA and optimal MSD; (c) Learning curves of the DF-APA in training and tracking modes.

Adaptive Filtering Attains Near-Optimal BER: To understand if adaptive symbol detection will suffice, we, in Fig 7.(b), compare the performance of the DF-APA suboptimal detector and the optimal detector MSD in minimizing the detrimental ISI effects caused by the vibrations as well as in increasing the average BER at a bitrate of 20 Mbps. Moreover, we study the effect of the number of tap weights employed in the FF and FB filters in DF-APA (Fig. 7(b)) on improving the system performance. We used step size μ=0.0005 to plot the BER diagrams associated with the DF-APA detector. As shown in Fig. 7(b), DF-APA is able to achieve a performance close to that of the MSD optimal detector with a window length N=4 by employing 6 tap weights in the FF filter (N_{FF}=6) and 3 tap weights in the FB filter (N_{FB}=3) at a much lower computational complexity.

An appropriate step size is critical for DF-APA detector in order to attain a good convergence speed and stability. Fig. 7(c) illustrates the relationship between the Mean Squared Error (MSE) by DF-APA and training sequence (d_k in training mode and $\tilde{d}_k$ in tracking mode) length in both training and tracking modes, where the number of gain taps in the detector's FF and FB filters are 6 and 3, respectively. To depict the learning curve, the expression $J(n) = |d_k - \hat{d}_k|^2$ in the training mode and $J(n) = |\tilde{d}_k - \hat{d}_k|^2$ in the tracking mode are computed from the detector's output, and after 1,000 times of running, the mean value of the results are obtained. As seen, $J(n)$ converges after about 1,500 iterations of updating the filter coefficients $\underline{\omega}$(n). Looking at various step sizes, the higher the step size (red and purple curves), the faster DF-APA finds the best coefficient configuration for symbol detection. However, higher step sizes may cause the filter going into potentially unstable operation. Fig. 7(c) shows that for step sizes $\mu \leq 0.01$ the DF-APA filter is stable. In particular, after about 300 iterations, all step sizes in both modes result in sufficient improvement in the learning curve and converge.

VII. Conclusion

We investigated the design of a VLC system with capability of data communication up to 20 Mbps over a 7.1 m distance. We considered vibrant and non-vibrant indoor VLC links. By deploying the prototype, we experimentally studied the detrimental effects of intense vibrations in the receiver's structural body on the VLC channel impulse response and integrity of the received signal. Furthermore, for reducing the ISI and adapt to the time varying nature of the vibrant VLC link and increasing the receiver's performance, we exploited optimal MSD and sub-optimal adaptive DF-APA detectors. Remarkable performance improvement was achieved by deploying the optimal MSD detectors within the vibrant VLC links but with exponential time requirements, and comparable improvements were obtained by the suboptimal DF-APA algorithm in polynomial time.

VIII. Acknowledgment

This work was supported in part by U.S. National Science Foundation awards 1836741 and 1663764.

References

[1] S. I. Mushfique and M. Yuksel, "Optimal multi-element VLC bulb design with power and lighting quality constraints," in Proceedings of ACM MobiCom Workshop on VLCS, 2016, pp. 7-12.

[2] Mengmi Zhou,Minglun Zhang,Yangan Zhang,"Design and implementation of long distance Visible Light Communication system based on Embedded ARM platform," Appl.Mech.Mater.(2014) 643646.

[3] M. V. Jamali, P. Nabavi, and J. A. Salehi, "MIMO underwater visible light communications: comprehensive channel study,performance analysis, and multiple-symbol detection, IEEE Transactions on Vehicular Technology, 2018.

[4] P. Gupta and P. R. Kumar, "The capacity of wireless networks," IEEE Transactions on Information Theory, vol. 46, 2000.

[5] A. Liu, J. Li, G. Shen, C. Sun, L. Li, and F. Zhao,Enabling low-power duplex visible light communication,arXiv preprint:1801.09812, 2018.

[6] Pure Lifi corporate, chief executive scientist: Professor Harald Haas FRSE, "https://purelifi.com/lifi-products/".

[7] Thorlabs, Part number: PDA36A2, "https://www.thorlabs.com".

[8] S. Park, D. Jung, H. Shin, D. Shin, Y. Hyun,K. Lee, and Y. Oh, "Information broad casting system based on visible light signboard,"Proceedings of the Wireless and Optical Communications," Canada, vol. 30,2007.

[9] Jie-Hui Li and Xing-Xing Huang and Xin-Ming Ji and Nan Chi and Jian-Yang Shi," An integrated PIN-array receiver for visible light communication,"Journal of Optics, vol. 17, no. 10, 2015.

[10] C. B. Yahya, "Design of wideband low noise transimpedance amplifiers for optical communications," in Proceedings of the 43rd IEEE Midwest Symposium on Circuits and Systems(Cat.No.CH37144), vol. 2, 2000.

[11] E. T. Won, D. Shin, D. Jung, Y. Oh, T. Bae,H.-C. Kwon, C. Cho, J. Son, D. O'Brien, T.-G.Kang, and T. Matsumura, IEEE P802.15Working Group for Wireless Personal Area Networks (WPANs): Visible Light Communication: Tutorial, 2018.

[12] Y. V. Zakharov, "Low-complexity implementation of the affine projection algorithm,"IEEE Signal Processing Letters, vol. 15, 2008.

[13] M. L. B. Riediger, R. Schober, and L. Lampe, "Fast multiple-symbol detection for free-space optical communications,"IEEE Transactions on Communications, vol. 57, no. 4, pp. 1119-1128,April 2009.

[14] K. Kiasaleh, "Performance of apd-based, ppm free-space optical communication systems in atmospheric turbulence,"IEEE Transactions on Communications, vol. 53, no. 9, pp. 1455-1461,Sept 2005.

[15] B. Farhang-Boroujeny,Adaptive filters: theory and applications. John Wiley and Sons, 2013.